

Beam Patterns of Low Frequency Radio Antennas using LEO Satellites

Paul Ries

September 21, 2007

Chapter 1

Introduction

Power patterns are fundamental to radio astronomy. Every antenna or array of antennas is designed with a specific sort of pattern in mind, usually one which is sensitive only in a narrow direction. Unfortunately, human manufacturing techniques are imperfect. Furthermore, even if an antenna were built exactly according to design, no antenna can do radio astronomy from inside an anechoic chamber, and thus the placement of the antenna in the field can also have unintended consequences. Side lobes or holes in the pattern could result. Thus a need arises for a way of determining the power pattern of an antenna in the field.

Traditionally, power patterns have been examined in the field by using calibrator sources such as the sun, CasA or other bright radio sources. However, these sources only traverse a limited range of sky and require that the telescope in question be steered.

The solution is to find an object that goes through most of the known sky. No astronomical object fits this description, but artificial satellites in low Earth orbit (LEO) do over the course of many passes. The best satellites to use for calibration of low frequency bands are the 37 satellites which are operated by Orbcomm corporation. These satellites transmit a near constant signal in the 137-138MHz band, which is near the frequencies used by low frequency arrays (e.g. those probing the epoch of reionization). In addition, over the course of several days, the satellites will make passes over all of the sky except for an $\approx 45^\circ$ radius hole centered on the north horizon. This hole is due to the inclination of the satellites' orbits and could be remedied by supplementing data from the Orbcomm satellites with observations of polar orbiting satellites operating in the same band.

Chapter 2

Sources of Error

2.1 Faraday Rotation

2.1.1 Expected Faraday Rotation

Faraday rotation is a phenomenon in which a polarized signal is “rotated” as it passes through an ionized medium. In the case of the Earth, this ionized medium is the ionosphere. The signals from the satellites are circularly polarized. Although a rotated circle is still a circle, the signals from the satellites gain an appearance of polarization due to fact that the antenna is pointed at the center of the Earth and not the observer. Figure 2.1 shows the crux of the matter. The angle, θ will cause the circularly polarized radiation to be projected into an ellipse depending on ϕ , which is simply $90^\circ + \text{elevation}$. The resulting equation for θ (assuming a typical satellite altitude of 800km) is

$$\theta = \sin^{-1}(6378/7178 * \sin \phi) \quad (2.1)$$

The fractional effect can be calculated by taking the cosine of θ . Faraday rotation can be calculated from the following formula:

$$RM = \frac{e^3}{2\pi m_e^2 c^4} \int_0^d n_e ds \quad (2.2)$$

All of this equation is a physical constant, except for the term inside the integral. The result of the integral is the column density of electrons. If we assume that the slant count is the same as the $\frac{N_e}{\sin alt}$, then we get the relation:

$$RM = 2.62 \times 10^{-5} \cdot \frac{TECU}{\sin alt} \quad (2.3)$$

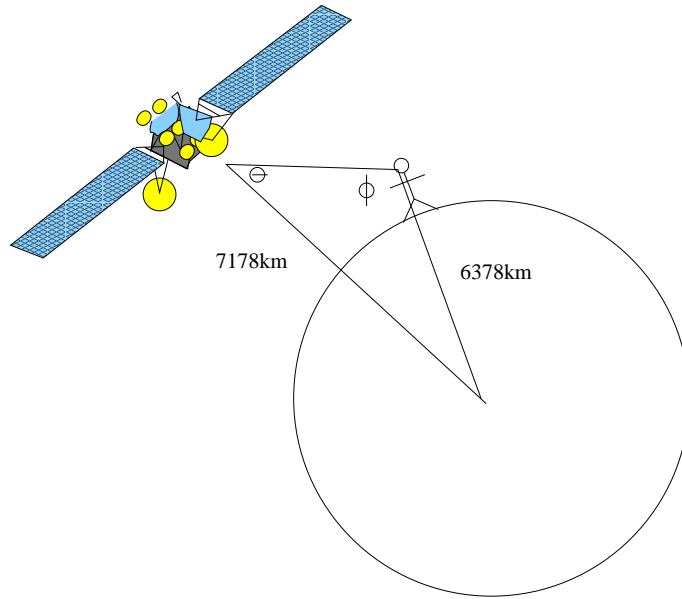


Figure 2.1: Satellite look angle

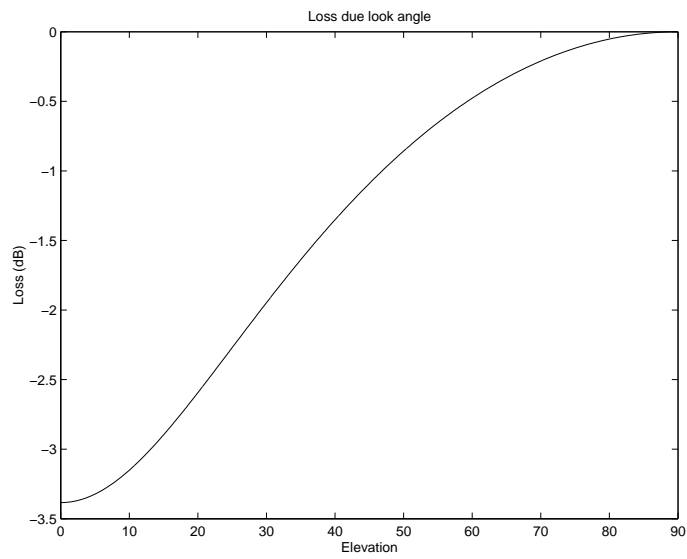


Figure 2.2: Maximum loss due to polarization/Faraday Rotation

Where the TECU is the total electron count in units of $10^{16}e^{-m^{-2}}$ The actual angle of rotation, β , can be calculated using the following equation:

$$\beta = RM \cdot \lambda^2 \quad (2.4)$$

at frequencies of 137.5 MHz, an angle of 40° above the horizon, and a TECU of 1-30 (possible range at site):

$$\begin{aligned} \lambda &= \frac{c}{\nu} = 220cm \\ \sin 40^\circ &= 0.64279 \\ \beta &= 2.62 \times 10^{-5} * 220^2 \cdot \frac{TECU}{0.64279} \\ &= 1.97 - 59.164rad \\ &= \frac{1}{3} - 10rotations \end{aligned}$$

2.1.2 Effect on Data

The effect of slant angle and Faraday rotation versus satellite altitude is plotted in figure 2.2.

Faraday rotation therefore can induce a loss of up to 3dB. This loss actually tends to more resemble “noise” in the data. The total electron count can vary from 1-30 TECU over the course of a single day, and the official NOAA electron count data is only rated to $\pm 1TECU$, or $1/3$ of a revolution. This uncertainty means that the rotation cannot be predicted and accounted for, since only a quarter of a revolution would completely shift the dropoff from one polarization for another. Therefore, we expect scatter to increase as the satellite moves farther from zenith.

2.2 Satellite Powers

A significant problem in this experiment is dealing with the fact that the satellites do not operate at the same power level. For undetermined reasons, the transmitted power from satellites of the Orbcomm constellation of satellites appears to vary by a factor of almost an order of magnitude.

The difficulty in solving this problem arises from trying to determine a common location that the satellites would eventually pass through. The data in all of the power plots, such as Fig. 4.2 shows an “edge” where satellites never cross, but all eventually pass through. This edge seemed like an ideal choice for comparing the satellite powers.

In order to find this orbit, a crude version of the PREDICT algorithm, which generates azimuth, elevation, and range from orbital elements and site information, had to be implemented based on the algorithms of Val-lado (2001). Through careful analysis, the shape of the pass was found to depend only upon the local hour angle between the right ascension of the ascending node of the orbit and the local sidereal time. Local sidereal time was adjusted in order to replicate the hole shape seen in the power plots. A single orbit did not produce the hole in the beam pattern. Instead, it turned out the edge of the hole was determined not by one orbit, but a series of orbit. However, only one type of orbit determined the minimum altitude at which satellites would cross the northern horizon. This orbit was determined to cross the horizon near azimuths of 270° and 90° and give a minimum altitude of around 42° at an azimuth of 0° . Fig. 2.3 shows the critical orbit and two orbits 20° different in local sidereal time to illustrate how multiple orbits lead to the edge in the data.

Orbits that fell within ten degrees of the predicted rise and set points and 3 degrees of the predicted transit altitude were flagged in order to compare the power of the satellites as they transited the northern meridian. Each pass on this orbit was fit with a quadratic curve on the points between azimuths of 355° and 5° . The intercept of this quadratic curve (i.e. the power level when transiting the meridian) was then used as the power level of the satellite. The resulting satellite powers can be found in Fig. 2.4.

These powers were taken into account later within the data analysis. Unfortunately, the power recorded for each satellite varied somewhat on each different pass during which it was measured. This difference may be due to changes at the satellite, gain variations in the receivers, or Faraday rotation. Unfortunately, these variations cannot be easily accounted for and therefore they remain a source of error at about the 5-10% level in voltage.

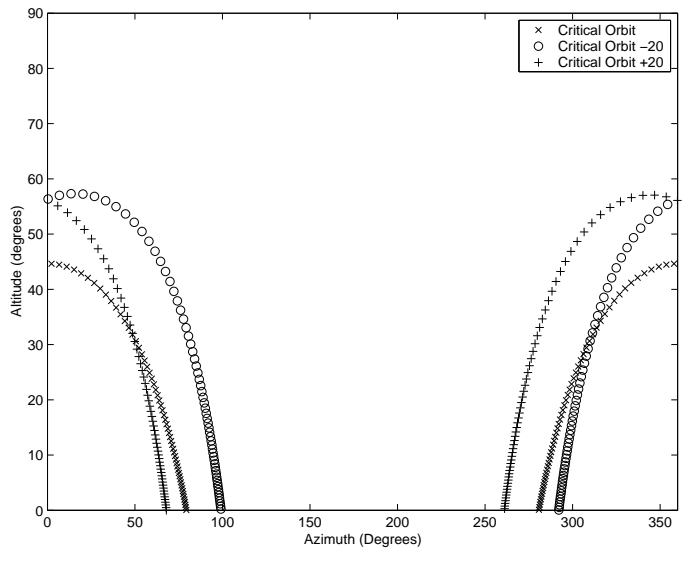


Figure 2.3: Critical Orbit

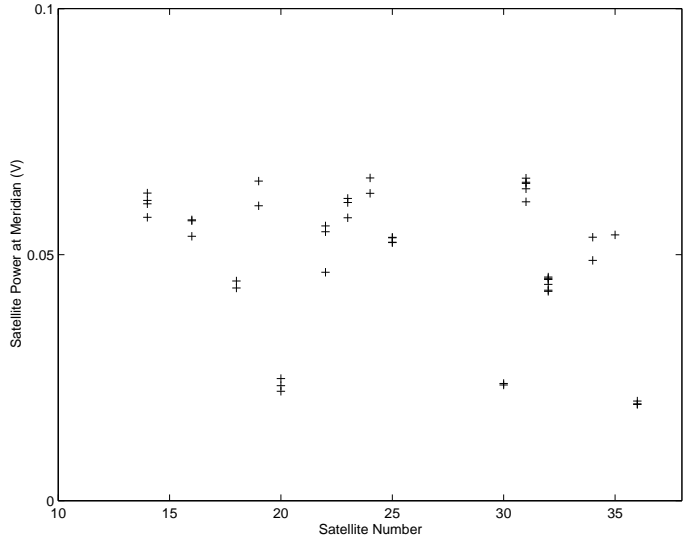


Figure 2.4: Satellite Powers. Note that multiple observations for each satellite were separated in time by about a day

Chapter 3

Power Measurements

3.1 Instrumentation

Figure 3.1 shows the overall experimental setup. The main goal of the system was to measure the intensity of the satellite power in two different polarizations.

The antenna used in this experiment was a very simple dipole and is pictured in Fig. 4.3 and elsewhere.

One polarization had data fed through a bandpass filter centered at 137.5 MHz and the other was sent through a high pass filter at 139 MHz. These filters were used to filter out RFI, primarily from the FM radio bands.

Each receiver consisted of two mixers, numerous amplifiers, and a saw filter. The first local oscillator was set to 732.1MHz in order to pump the 137.5 MHz frequency of the satellites to the center of the saw filter at 869.6 MHz. The second LO at 871.1MHz brought the frequency down to the IF output of the receiver around 1.5 MHz, making the net mixing effect equivalent to a single LO at a frequency of 139 MHz. The net gain of the receivers was approximately 30dB.

The IF output was then connected to a PC9812 PCI data acquisition card (DAC). This card had 5 channels of input, four for data, one for a trigger/clock signal. The clock signal came from a signal generator operating at 8.192MHz. Each receiver used one of the inputs on the data card, leaving two unused ports for future experiments. A 1.5 MHz test signal was used when only one channel was in operation in order to verify the integrity of the 2 channel software.

3.2 Data Acquisition

Data was acquired near the Interferometer Control Building at the NRAO in Green Bank, WV from June 9 through June 17. During that time, 546 individual satellite passes were observed. Satellite orbit data was generated using the Linux program *predict*. The computer taking the data was also equipped with Network Time Protocol, as time errors of greater than one second were shown to significantly increase systematics in the data.

3.3 Data Reduction/Calibration

The data acquisition program recorded data consisting of 256 voltage bins. This data is equivalent to covering frequencies between 137 and 138MHz in 4 kHz intervals. These files were recorded in a binary format, along with information on which satellites were overhead at the time the data was recorded.

This raw data was fed into a program that checked frequencies known to harbor satellites for the presence of that satellite when it was known to be overhead. A "pass file" was then generated which contained the altitude, azimuth and range of the satellite at the time of observation and the voltage at that particular frequency from both of the input channels.

A number of calibrations had to be performed to turn the raw voltages from the receivers into useable data. One issue that clearly needed to be tackled was correcting for the range of the satellites. However, this was fairly trivial to do, as the range of the satellites was already recorded by the *getsatdat* program. Using the fact that power falls off as $\frac{1}{r^2}$, the satellites were corrected to the power that should have been received from reference altitude of 800km.

The relative powers of the satellites were obtained by the method described earlier or tweaked by hand to make for a more uniform map. This source of error was corrected by multiplying by the ratio of each satellites expected voltage to an arbitrary reference voltage.

One last but critical required calibration was the subtraction of bias/noise from each pass. Initially, this step was not seen as important. However, when the range correction was first applied, power at the horizon appeared stronger than at the zenith, which is not a physical result. The satellites are at the largest distance near the horizon and have the largest range correction. At the same time, the satellites have the lowest signal to noise ratio, and thus the noise becomes extremely amplified. This bias was removed by

taking a 20 point average of both the first and last points of each pass, taking the lowest of these two averages, then subtracting from the total power. Two averages are required in the event that a pass does not start and end near the horizon, such as at the beginning or end of a data file.

The final correction applied was:

$$V_{cal} = (V_{obs} - V_{bias}) \cdot \frac{r_{sat}}{r_{ref}} \cdot \frac{V_{ref}}{V_{sat}} \quad (3.1)$$

All of this data was then rolled into a map with pixels corresponding to $0.1^\circ \times 0.1^\circ$. This $0.1^\circ \times 0.1^\circ$ map was then averaged over a ten pixel by ten pixel box and formed into a $0.5^\circ \times 0.5^\circ$ map of voltage against position over the entire sky.

3.4 Results

Figure 3.2 shows the overall beam map from the ICB site with terrain overlaid. The most obvious phenomenon shown by the map is the direct blocking of signals by the terrain. The radio dish at 80° azimuth and the mountain range in the west both fit the data nicely. The other obvious result is that the beam is fairly clean. Visual inspection shows no obvious side lobes. In fact, the only visible feature of the antenna beam pattern is the dropoff centered near zero elevation and 190° of azimuth that corresponds to the direction the dipole is pointing.

One fascinating feature of this diagram is that all of the antennas (both the dipole and various PAPER antennas) measured by this experiment in several different locations around NRAO Green Bank all were pointing in the wrong direction! The minimum corresponding to the dipole is at 190° azimuth, but the antenna was aligned using an orienteering compass on true north. The minimum should have been at 180° , implying the antenna was misaligned by 10° . Although the magnetic variation at the site is close to 10° , this variation was already accounted for when aligning the antenna. The source of this unexplained anomaly is most likely either a local magnetic anomaly in the Green Bank area, or very localized variation due to the nearly identical groundscreens used on the antennas. Both explanations would apply to all the antennas.

A CST simulation for the simple dipole was available and a meaningful comparison could be made with the overall shape of the beam. Figures 3.3 and 3.4 show the planes perpendicular and parallel to the dipole, respectively. In the perpendicular plane, the simulation and observation are in

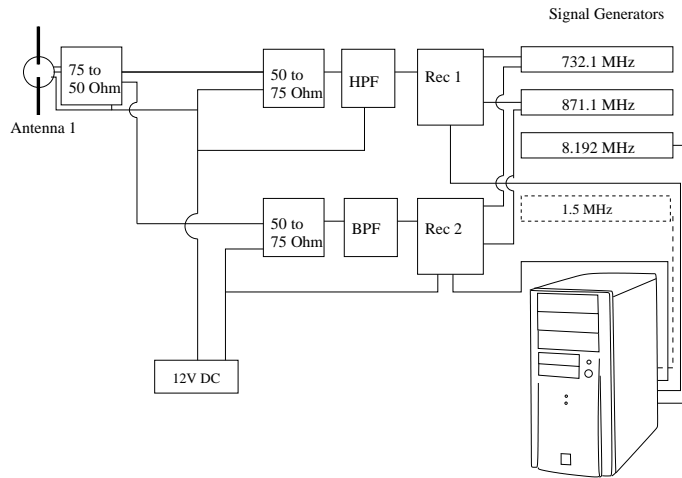


Figure 3.1: Block Diagram of Power Measurement system

good agreement. The observations fall off steeper within 10° of the horizon, but that is easily explained by the presence of various obstructions at that elevation. The case of the parallel plane is somewhat more interesting. A drop-off is still present at low elevation; however, this drop-off is much more pronounced and begins at a much higher elevation. In addition, the observed power drops off more quickly on the right than on left.

The more rapid drop-off on the right side of Fig 3.4 is easily explained by the existence of some moderately tall obstructions in that section of the sky. Although some of the fall-off is due to obstructions near ground level, none of these obstructions extend up to the $\approx 30^\circ$ of elevation where the drop off begins. Therefore, the explanation must lie in the beam pattern of the antenna itself. The most likely explanation is that the conductivity chosen for the ground may be incorrect in the CST model used for comparison. Intriguingly, a more conductive ground could also explain the magnetic anomaly mentioned earlier, but the evidence is far from conclusive.

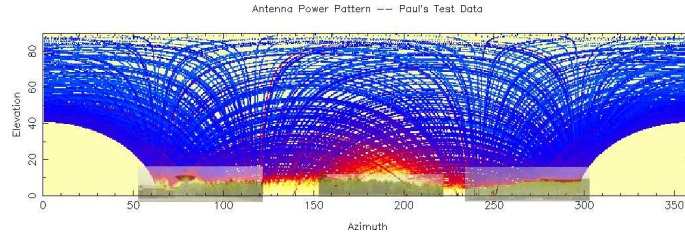


Figure 3.2: Overall power pattern of a N-S dipole at the ICB site. Overlaid are important terrain features to scale. The influence of these features is quite prominent near the horizon. White shows lowest intensity and blue shows the highest.

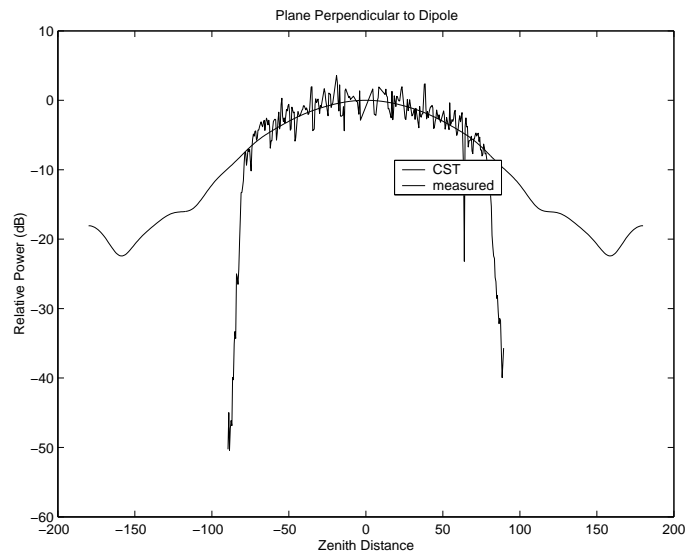


Figure 3.3: Power pattern of Antenna in the plane perpendicular to the axis of the dipole. A CST Microwave studio model and model obtained with satellites in the field are shown.

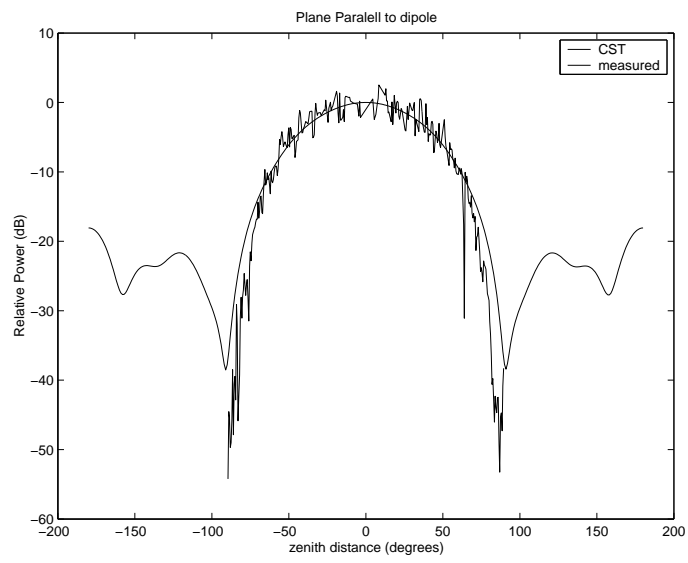


Figure 3.4: Power pattern of Antenna in the plane paralell to the axis of the dipole. A CST Microwave studio model and model obtained with satellites are shown.

Chapter 4

Difference Measurements

4.1 Instrumentation

Figure 4.1 shows the system used for the difference measurements. Essentially, the setup was very similar to that used by the power measurement system described previously. Instead of measuring two polarizations from one antenna, one polarization was measured from two different antennas.

The antennas used for this experiment were simple dipoles with an active balun with about 15 dB of gain. Each antenna was placed on a mast atop a groundscreen. These antennas were spaced approximately 30 ft. apart along an approximately North-South axis.

The cables between the impedance matching circuits were 230 ft and 500 ft in length for the two antennas. These cables were 75Ω cables. All other cables used were 50Ω cables.

4.2 Data Acquisition - ICB

Data was acquired from July 6-9 on the radio astronomy reservation in Green Bank, WV. The end result was 272 passes from more than a dozen satellites. Two antennas were used in the hope that the end result would be null. That is to say, in an ideal world, two identical antennas measuring the power from an identical satellite from almost identical positions on Earth should record identical powers, or powers different by a constant systematic factor.

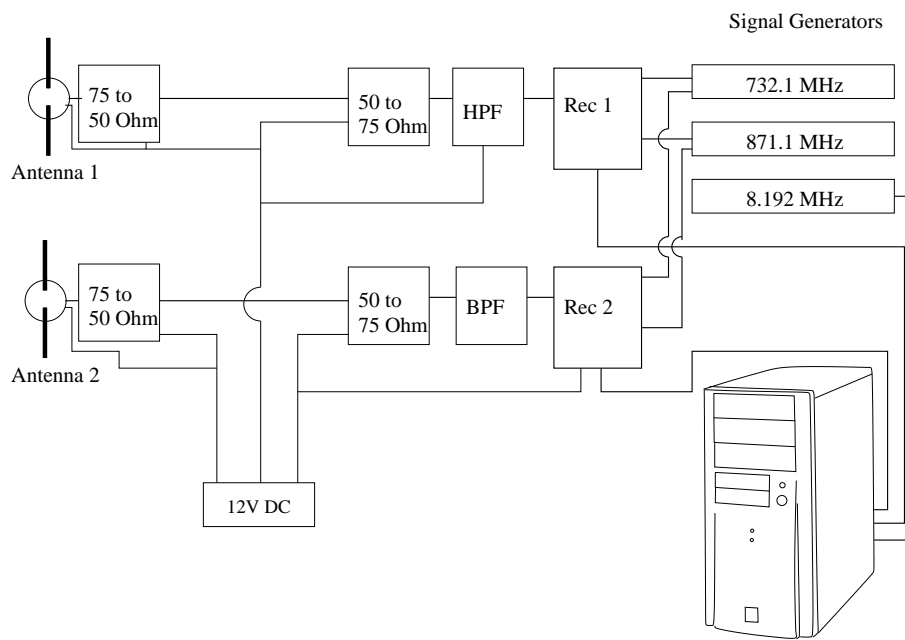


Figure 4.1: Block Diagram

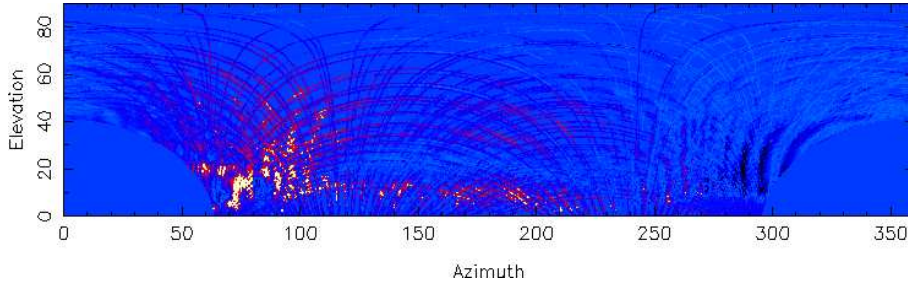


Figure 4.2: Percent difference between the two antennas. Red to white represents a positive difference; light blue-black are used to represent a negative difference.

4.3 Data Acquisition - PAPER site

Two runs of data were also taken at the PAPER site in Green Bank using PAPER antennas sporadically during August 2007 over a total of about four days.

4.4 Data Reduction

The data reduction was nearly identical to that used in the power measurements. However, all of the corrections for bias, range, and satellite powers were dropped, since the whole point of the difference measurement was to remove those sources of error.

The main difference came in computing the final all-sky map of the beam. Rather than computing power in two polarizations, the difference between each channel in the map was computed using the formula:

$$\%Difference = \frac{2 * (V1 - V2)}{V1 + V2} \quad (4.1)$$

4.5 Data Analysis - ICB

Figure 4.2 shows the difference between the two antennas. The maximum deviations were -59% and $+44\%$ in voltage. The results were not anywhere near the null that we had expected. Furthermore, the results were clearly dominated by systematic, rather than random features.



Figure 4.3: The tower believed to responsible for vertical fringes

This figure shows four dominant features. The strongest feature, percentage-wise, occurs between the azimuths of 65° and 90° and altitudes of 0 and twenty degrees. These deviations are clearly the results of an 85 ft antenna and a building at those azimuths, and the parallax due to the different locations of the two antennas.

The next largest feature spans almost the entire map; however, this error is most obvious between the azimuths of 240° and 360° degrees. One can easily observe what appear to be vertical fringes. While these fringes are less obvious in the southern part of the sky, careful examination of the data shows that they are still present. These fringes are significant at about the 10% level in voltage and 1% level in power. The source of these fringes appears to be the tower depicted in figure 4.3. This tower stretches approximately 40° in elevation from the antenna site, and sits at an azimuth of around 10° , which seems to correspond with the origin of the fringes in figure 4.2. Scattering off this tower appears to be responsible.

The third feature is the enhancement at an elevation of 25° in most of the southern half of the sky. A decrement also appears at the same azimuths about ten degrees below. The most likely culprit is the cable housing for the old NRAO interferometer range, visible in figure 4.4. As above with



Figure 4.4: A long cable housing believed to be responsible for the observed horizontal fringes

the tower, scattering again appears to bear the responsibility for the fringes, which are of order slightly less than 1% in power. The cable housing is the chief suspect since it extends from almost exactly the same azimuth that the fringe does.

The fourth and final pattern visible in this plot the enhancement in the northwest and the decrement in the southeast. This error most likely results from a warp in the ground screen of one of the antennas. One antenna has a visibly flat groundscreen, however, the other one has a significant depression of the groundscreen in the southeast quadrant of the groundscreen as visible in figure 4.5. This depression (most likely caused by an errant grad student) would be expected to steer the beam of the northernmost telescope towards the southeast, which would make it less sensitive in the northwest and more sensitive in the southeast. This effect also occurred at about the 1% level.

4.6 Data Analysis - PAPER site

The results from the PAPER site were much less enlightening. For some reason, the PAPER antennas generated much more noise than did the simple dipole. The source of this noise may have been cable wear or the fact that the balun had less gain than the one used in the simple dipole. The end result was that there was only one feature in the data from the PAPER site that could not be chalked up to variation between the two antennas. Fig. 4.6 shows a difference map at this site. The one feature that is real is the blob between 100° and 200° of azimuth. In fact, it almost looks like a fringe



Figure 4.5: Antenna and groundscreen. Please note the warp in the nearest quadrant of the groundscreen

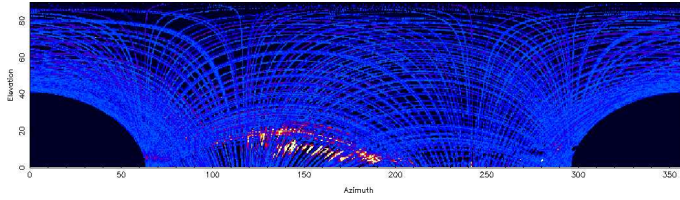


Figure 4.6: Difference map between two antennas at the PAPER site. Blue is a positive difference and white is a negative difference.



Figure 4.7: 360° panorama around the dipole believed to be experiencing fringing. Edges correspond approximately with NNE direction. Note the knoll in the SE.

due to scattering. From the point of view of one of the antennas, there is a rather sizeable knoll at that location, as can be seen in the panorama in Fig. 4.7. The top of the knoll had nothing metallic off which the signal could scatter, but not far on the other side of the knoll, a double fence was present. This fence is shown in Figure 4.8. The second antenna was located much farther away from the knoll.

Two factors indicate that the fence may not be the answer. First, there is the fact that the topmost fringe is at almost the same elevation as the peak of the knoll. Conceivably, the “fringes” could just be the result of the hill blocking the signal to one of the antennas. The section of the fringe where there is an increase in signal where the hill should be blocking can be explained by the fact that the satellite signals are very weak in that section of the sky. The second factor is the fact that the fence is definitely well over the crest of the hill, such that it was not immediately obvious for an observer standing at the top of the thickly-wooded hill. The position of the fence yields a high probability that any scattering off the fence would be blocked by the intervening hill.

4.7 Discussion

Overall, these results are very promising. Except for the parallax effect, none of the effects observed by using the reference antenna was expected. Furthermore, testing in an anechoic chamber would never have produced any of the effects either.



Figure 4.8: The fence that may be responsible for the fringes observed in figure 4.6

A few questions, however, remain. For instance, while scattering can be seen to produce fringing in one or both antennas, why it produces fringing in the difference is unclear. Both antennas should show fringing, but in slightly different locations. The fringes visible in Figure 4.2 may in fact be the superposition of fringes from the two antennas.

Another unanswered question is how one determines the in-situ beam pattern of a single antenna. While the satellite method can work for this, it is severely limited by systematic errors that are difficult to control (see discussion above). Once the pattern of a single antenna is established, however, that antenna can be used as a reference antenna for any other antennas in an array or for an array as a whole.

Chapter 5

Future Research

5.1 Observing Faraday Rotation

Although Faraday rotation was treated as a source of noise in the measurements obtained here, these Orbcomm satellites actually provide an opportunity for high precision characterization of Faraday rotation. At 137.5 MHz, signals are very sensitive to Faraday rotation. Faraday rotation is normally measured from GPS satellites operating in the 2 GHz range, which are much less sensitive to changes in the electron content of the atmosphere. One possibility for a future project would be to simultaneously measure the electron count using one of the Orbcomm satellites and one of these GPS satellites. The GPS satellite would yield a coarse value of the electron count and the Orbcomm satellites would yield a fine value, perhaps more accurate than has been obtained in the past.

5.2 Better reference antenna

While the simple dipole used for some of these measurements has strong signal and a clean beam, it had several drawbacks that could be improved upon in the future. The main issue is that the antennas are very flimsy and prone to damage. For instance, grabbing the antenna by the the dipole elements could easily shift the position of the element or snap the wire that connects it to the balun. One improvement implemented over the course of this experiment was to attach balsa shims to each dipole element to prevent them from sliding or rotating, but this improvement is only a temporary measure. A sturdier antenna would greatly improve the experiment as it could be used as a reference antenna for many future difference experiments.

5.3 Expanding the number of elements

The main justification for this project is its applicability to arrays of antennas which are difficult to impossible to measure for beam patterns in a laboratory setting. A number of designs are currently under consideration (PAPER, FASR, SKA, MWA, Lofar) which would have many dipoles laid out over many kilometers. This method of using LEO satellites to determine beam patterns in the field could easily be extended to arrays. Since these arrays will not fit in any anechoic chamber in existence, the satellite method is a viable alternative to using celestial sources and provides additional benefit with the large fraction of the sky covered.

Chapter 6

Conclusion

This experiment has shown numerous applications of LEO satellites to the beam patterns of low frequency radio instruments. This project demonstrated the viability of using satellites to determine the overall beam pattern of low frequency antennas. This project also showed numerous instances where nearby buildings and objects caused deviations across almost the entire beam due to scattering. Furthermore, the alignment of a number of antennas was discovered to be faulty. This method clearly shows promise for aiding in the setup and calibration of future low frequency radio arrays.